Recent Advances in Performance-Driven Surrogate Modeling of High-Frequency Structures

Slawomir Koziel and Anna Pietrenko-Dabrowska

Engineering Optimization & Modeling Center
Reykjavik University, Reykjavik, Iceland
(koziel@ru.is)
Faculty of Electronics, Telecommunications and Informatics
Gdansk University of Technology, Gdansk, Poland
(anna.dabrowska@pg.edu.pl)

Abstract

Design of high-frequency structures, including microwave and antenna components, heavily relies on full-wave electromagnetic (EM) simulation models. Their reliability comes at a price of a considerable computational cost. This may lead to practical issues whenever numerous EM analyses are to be executed, e.g., in the case of parametric optimization. The difficulties entailed by massive simulations may be mitigated by the use of fast surrogates, among which data-driven models are the most popular ones due to their versatility and accessibility. Unfortunately, conventional modeling techniques are significantly affected by the curse of dimensionality. It is particularly restrictive in the case of high-frequency components, typically exhibiting highly nonlinear characteristics. Recently, the concept of performance-driven modeling has been proposed where the surrogate model setup is focused on a small subset of the parameter space, containing the designs that are optimal or nearly optimal with respect to the considered performance figures. Domain confinement allows for a dramatic reduction of the number of training data samples needed for rendering reliable surrogates valid over wide ranges of the system parameters. In this paper, we review some of the recent techniques employing these concepts, discuss their properties, and illustrate them using real-world examples of antenna and microwave components.

1. Introduction

Over the years, design of modern high-frequency structures has been increasingly dependent on full-wave electromagnetic (EM) analysis tools. EM simulation packages entered the level of sophistication that permits reliable evaluation of arbitrary geometries while taking into account various effects such as cross-coupling between system components [1], dielectric anisotropy [2], or the presence of installation fixtures and radomes [3]. It is a fact of the matter that the complexity of contemporary high-frequency devices leads to making larger and larger portions of the design process EM-driven. This is especially pertinent to parameter tuning. At this stage of the process (also referred to as design closure [4]), the system performance is to be improved by finding the best possible trade-off between conflicting objectives while satisfying the design constraints. Adjustment of the parameters is typically carried out using numerical optimization procedures, which entails considerable computational expenses being a result of multiple EM simulations involved. This is one of the major challenges pertaining to EM-based design processes. It can be aggravated by solving tasks such as global optimization [5], uncertainty quantification [6] or robust design [7], all of which require massive evaluations of the structure at hand.

Mitigation of the cost issue has been addressed by a number of researchers over the last two decades or so [8]-[11]. At the level of numerical algorithms, possible remedies rely on the development of more efficient procedures. The two notable directions are incorporation of the adjoint sensitivity technology to accelerate gradient-based search procedures [12], [13], as well as (local) surrogate-assisted methods [14]-[16]. Among the latter, one of the most recognized techniques is space mapping [17].

Other frameworks include response correction methods [18], [19], feature-based optimization [20], or combination of surrogates with machine learning algorithms [21]. Majority of the aforementioned approaches shift some (or most) of the computational burden into cheaper representations of the structure under design while occasionally referring to the original (high-fidelity) EM model for verification and upgrading the (usually local) surrogate.

Replacing the high-fidelity model by its faster surrogate altogether is an attractive alternative to the methods mentioned in the previous paragraph, as it permits a rapid execution of all types of simulation-based design procedures. Among available modeling techniques, the data-driven surrogates belong to the most popular ones due to their versatility and availability [22]-[25]. These surrogates are constructed by approximating the data from the original (here, EM-simulated) model of the system of interest. No physical or engineering insight is required. Some of widely used methods include polynomial regression [26], radial basis functions [27], kriging [28], support vector regression (SVR) [29], Gausian Process Regression (GPR) [30], or polynomial chaos expansion (PCE) [31] (typically in the context of uncertainty quantification); recent methods often incorporate combinations of the basic frameworks, e.g., PC kriging [32], where PCE is used as a trend function and the residuals are modelled with kriging.

Unfortunately, approximation models are severely affected by the curse of dimensionality [33], i.e., a rapid growth of the number of training samples necessary to ensure usable predictive power of the surrogate with the increase of the number of independent parameters and their ranges. For high-frequency structures, often characterized by nonlinear responses, construction of data-driven surrogates is typically

limited to a few parameters within narrow ranges thereof. This is insufficient to handle geometrically complex topologies of modern microwave and antenna components. Some methods designed to address the issues of conventional modeling methods include high-dimensional model representation (HDMR) [34], feature-based modeling [35], orthogonal matching pursuit (OMP) [36], as well as techniques for blending data of various fidelities, e.g., space mapping [37], Bayesian model fusion [38], co-kriging [39], or two-stage GPR [40].

Recently, a performance-driven modeling approach has been proposed, where the problem of an excessive cost of training data acquisition is addressed by an appropriate definition of the surrogate model domain [41]. The main concept stems from the observation that a vast majority of a conventional domain, normally determined by the lower and upper bound for the structure parameters, contains designs that are of poor quality from the point of view of any set of performance requirement that are of interest in a given design context. Confining the model domain to the vicinity of the region that accommodates optimum (or nearly optimum) points enables significant computational savings because only this region needs to be sampled and accounted for by the surrogate. In practice, determination of such a region is based on a set of reference designs pre-optimized with respect to the figures of interest of choice. The details depend on a particular technique. The initial attempts of performance-driven modeling were focused on constructing surrogates covering a particular range of operating frequencies. Extended versions allowed taking into account additional operating conditions (e.g., relative permittivity of the substrate the structure is implemented on [42]) while retaining a structured reference design set. Performance-driven modeling with arbitrary allocation of

the reference designs has been proposed in [43], further improved in the nested kriging framework which allows straightforward uniform domain sampling and surrogate model optimization.

This paper summarizes the recent developments and implementations of performance-driven surrogate modeling. We discuss three approaches, modeling with structured reference design set [41,42], triangulation-based modeling [43,44], as well as the nested kriging framework [45,46]. The presented methods are illustrated using real-world examples of microwave and antenna structures, and benchmarked against conventional surrogate modeling methods. A discussion of their advantages and disadvantages is also provided. The exposition of the techniques is preceded by a generic formulation of the performance-driven modeling concept.

2. Performance-Driven Surrogate Modeling

Here, a concept of performance-driven modeling is formulated at a generic level. In particular, we explain the distinction between the conventional surrogate model domain and the domain confined by the conditions imposed by the design optimality w.r.t. the considered performance figures. Practical realization of this concept using various methods is then discussed in Sections 3 through 5.

2.1. Parameter Space and Objective Space. Design Optimality

The parameter space of the high-frequency structure at hand will be denoted as X. It is defined in a usual way, i.e., using the lower and upper bounds on design variables $l \leq x \leq u$, where $x = [x_1 \ldots x_n]^T$, $l = [l_1 \ldots l_n]^T$, $u = [u_1 \ldots u_n]^T$, or $X = [l_1 \ u_1] \times \ldots \times [l_n \ u_n]$. The figures of interest considered throughout the design process will be denoted as f_k, $k =$

1, …, N. Examples of such figures include the operating frequencies of a multi-band antenna [41], material parameters (e.g., relative permittivity of the dielectric substrate the structure is implemented on [42]), or the power split ratio of a coupler [46]. The objective space F is defined by the ranges (lower and upper bounds) for the figures f_k, $f_{k.\min} \leq f_k^{(j)} \leq f_{k.\max}$, $k = 1, …, N$. In other words we have $F = [f_{1.\min} \ f_{1.\max}] \times … \times [f_{N.\min} \ f_{N.\max}]$. The design goals for a given target objective vector $\boldsymbol{f} = [f_1 \ … \ f_N]^T$ are encoded in a scalar objective function $U(\boldsymbol{x}, \boldsymbol{f})$, whereas the design optimality is understood as a solution to the problem

$$U_f(\boldsymbol{f}) = \arg\min_{\boldsymbol{x}} U(\boldsymbol{x}, \boldsymbol{f}) \tag{1}$$

Here, $U_f(\boldsymbol{f})$ denotes the design that is optimum with respect to the objective vector $\boldsymbol{f}$. For example, if $\boldsymbol{f}$ is a vector of operating frequencies of a multi-band antenna, $U(\cdot)$ may be defined as $-\min\{B_1, …, B_N\}$, where B_j is the fractional operating bandwidth corresponding to the operating frequency f_j. In that case, $U_f(\boldsymbol{f})$ will be a design that maximizes the antenna fractional bandwidths while allocating them at the required frequencies $\boldsymbol{f}$.

The image $U_f(F)$ of the objective space F is an N-dimensional manifold in the parameter space X as shown in Fig. 1. Whenever the figures f_k are of concern, $U_f(F)$ is the only region of X that is of interest because it contains the designs that are of high quality with respect to f_k as specified by the objective function U. When constructing a design-ready surrogate, it is sufficient to focus the model domain in and around $U_f(F)$, which allows for considerable computational savings in terms of training data acquisition as compared to rendering the model within the entire parameter space X.

Clearly, several practical problems arise: (i) how to identify $U_f(F)$, (ii) how to carry out design of experiments (training data allocation), and, finally, (iii) how to use the

surrogate for design purposes (e.g., parametric optimization) given geometrical complexity of the domain. These issues will be dealt with in Sections 3 through 5 when discussing particular realizations of the performance-driven modeling concept.

2.2. Performance-Driven Modeling Flow

Figure 2 shows the surrogate modeling flow according to the performance-driven approach. The critical stage is a determination of the surrogate model domain, which takes into account the objective space and performance figures therein. The information about allocation of high-quality regions of the parameter space is carried by the reference designs prepared beforehand. The major differences between various implementations of the modeling procedures is in the particulars of how this information is employed.

3. Performance-Driven Modeling with Structured Reference Design Set

The first implementation of the performance-driven modeling concept were characterized by a pre-defined allocation of the reference designs, which limits the flexibility of the framework. At the same time, these methods featured relatively straightforward formulation. The method outlined in this section was specifically developed to model the antenna structures with respect to the operating frequency and material parameters (relative permittivity of the dielectric substrate) [42].

3.1. Modeling Procedure

Here, the objective space is two-dimensional with the figures of interest being the operating frequency f and relative dielectric permittivity ε_r of the substrate. The surrogate model is to be reliable for the range of operating frequencies $f_{min} \leq f \leq f_{max}$, and the range

of permittivity $\varepsilon_{\min} \leq \varepsilon_r \leq \varepsilon_{\max}$. $\boldsymbol{R}(\boldsymbol{x})$ represents a response of an EM-simulated antenna model, where $\boldsymbol{x}$ is a vector of antenna parameters. The symbol $U_f(f, \varepsilon_r)$ will denote the design optimized for the operating frequency f and the substrate dielectric permittivity ε_r.

The surrogate model domain is defined as a vicinity of the manifold spanned by nine reference designs covering the aforementioned ranges of f and ε_r. These are $U_f(f^*, \varepsilon_r^*)$, for all combinations of $f^* \in \{f_{\min}, f_0, f_{\max}\}$ and $\varepsilon_r^* \in \{\varepsilon_{\min}, \varepsilon_{r0}, \varepsilon_{\max}\}$, cf. Fig. 3.
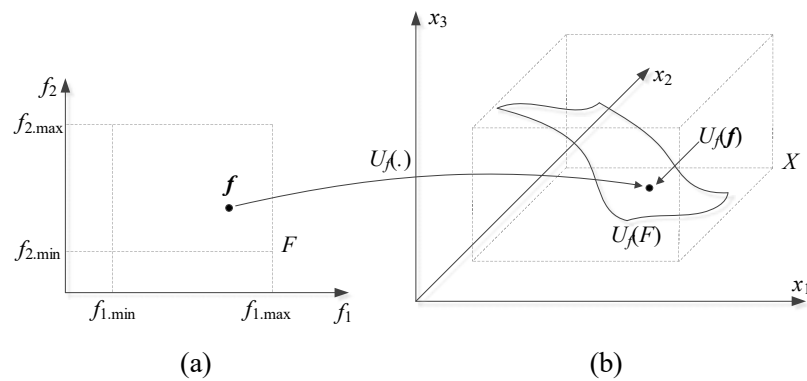

(a)   (b)

Fig. 1. Performance-driven modeling: (a) the objective space F (here shown for $N = 2$) and (b) the design space X (shown for $n = 3$). The image $U_f(F)$ of F is an N-dimensional manifold in X containing the designs that are optimal w.r.t. the figures of interest f_1 through f_N. From design perspective, the surrogate modeling process can be restricted to $U_f(F)$ [45].
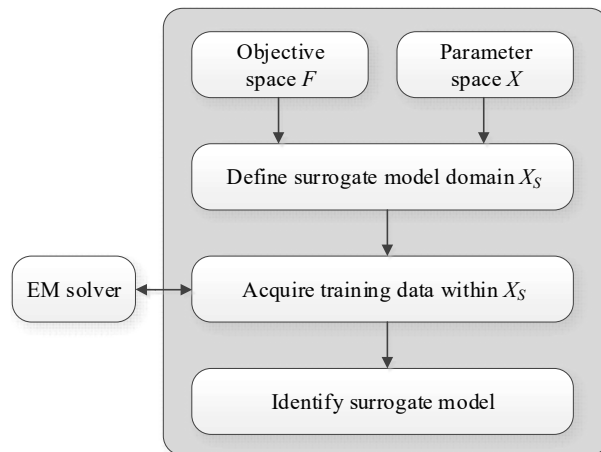

Fig. 2. Performance-driven modeling flow.

We define vectors $v_1 = U_f(f_{min}, \varepsilon_{min}) - U_f(f_0, \varepsilon_{r0})$, $v_2 = U_f(f_{min}, \varepsilon_{r0}) - U_f(f_0, \varepsilon_{r0})$, $v_3 = U_f(f_{min}, \varepsilon_{max}) - U_f(f_0, \varepsilon_{r0})$, $v_4 = U_f(f_0, \varepsilon_{max}) - U_f(f_0, \varepsilon_{r0})$, $v_5 = U_f(f_{max}, \varepsilon_{max}) - U_f(f_0, \varepsilon_{r0})$, $v_6 = U_f(f_{max}, \varepsilon_{r0}) - U_f(f_0, \varepsilon_{r0})$, $v_7 = U_f(f_{max}, \varepsilon_{min}) - U_f(f_0, \varepsilon_{r0})$, and $v_8 = U_f(f_0, \varepsilon_{min}) - U_f(f_0, \varepsilon_{r0})$, see Fig. 3(a). We also define a manifold M, which is spanned by eight pairs of vectors $[v_1, v_2]$, $[v_2, v_3]$, …, $[v_8, v_1]$, as [42]

$$M = \bigcup_{k=1}^{8} M_k = \bigcup_{k=1}^{8} \{ y = U_f(f_0, \varepsilon_{r0}) + \alpha v_k + \beta v_{k+1} : \alpha, \beta \geq 0, \alpha + \beta \leq 1 \} \tag{2}$$

For the sake of consistency, we define $v_9 = v_1$. Figure 4(b) shows a point z and its projection $P_k(z)$ onto the hyper-plane containing M_k. It corresponds to the expansion coefficients w.r.t. v_k and v_{k+1}:

$$\arg \min_{\bar{\alpha}, \bar{\beta}} \left\| z - \left[U_f(f_0, \varepsilon_{r0}) + \bar{\alpha} v_k + \bar{\beta} v_{k+1}^{\#} \right] \right\|^2 \tag{3}$$

where $v_{k+1}^{\#} = v_{k+1} - p_k v_k$ with $p_k = v_k^T v_{k+1} (v_k^T v_k)$. Thus, $v_{k+1}^{\#}$ is a component of v_{k+1} that is orthogonal to v_k. Consider

$$\left[v_k \ v_{k+1}^{\#} \right] \left[\bar{\alpha} \ \bar{\beta} \right]^T = z - U_f(f_0, \varepsilon_{r0}) \tag{4}$$

The least-square solution to (4) (equivalent to the solution of (3)) is given as

$$\left[\bar{\alpha} \ \bar{\beta} \right]^T = \left(V_k^T V_k \right)^{-1} V_k^T \left(z - U_f(f_0, \varepsilon_{r0}) \right) \tag{5}$$

where $V_k = [v_k \ v_{k+1}^{\#}]$. For practical reasons, we are interested in the expansion coefficients with respect to v_k and v_{k+1}, which are given as $\alpha = \bar{\alpha} - p_k \bar{\beta}$, $\beta = \bar{\beta}$. Note that $P_k(z) \in M_k$ if and only if $\alpha \geq 0$, $\beta \geq 0$, and $\alpha + \beta \leq 1$.

We define $x_{max} = \max\{ U_f(f_0, \varepsilon_{r0}) + v_1, \ldots, U_f(f_0, \varepsilon_{r0}) + v_8 \}$ and $x_{min} = \min\{ U_f(f_0, \varepsilon_{r0}) + v_1, \ldots, U_f(f_0, \varepsilon_{r0}) + v_8 \}$. The vector $dx = x_{max} - x_{min}$ is the range of variation of antenna

geometry parameters within the manifold M. The surrogate model domain X_S is defined as follows: a vector $y \in X_S$ if and only if

1. The set $K(y) = \{k \in \{1,\ldots,8\} : P_k(y) \in M_k\}$ is not empty;

2. $\min\{\|(y - P_k(y))//dx\| : k \in K(y)\} \le d_{max}$, where $//$ denotes component-wise division (d_{max} is a user-defined parameter, typically between 0.1 and 0.2).

The first condition ensures that y is sufficiently close to M in a "horizontal" sense. In the second condition, the normalized distance between y and its projection onto that M_k, to which the distance is the shortest, is compared to the user-defined d_{max}. Due to normalization w.r.t. the parameter ranges dx, d_{max} determines the "perpendicular" size of the surrogate model domain (as compared to the "tangential" size given by dx).

By definition, all the reference designs and the manifold M belong to X_S. The size of X_S is dramatically smaller (volume-wise) than the size of the hypercube containing the reference designs (i.e., x such that $x_{min} \le x \le x_{max}$).
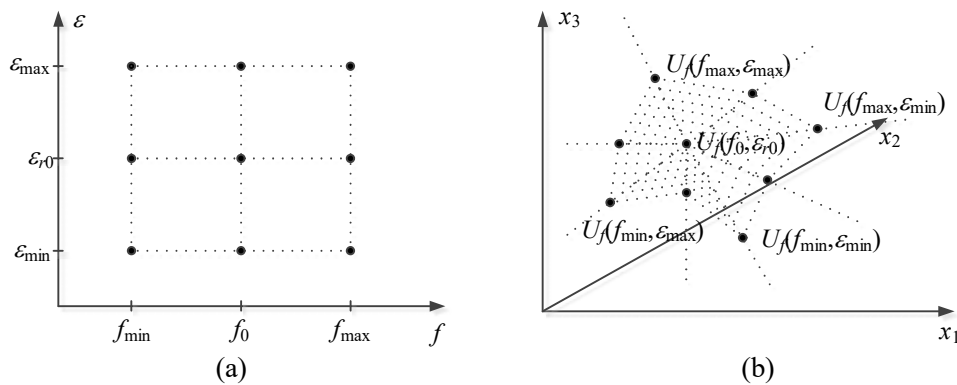

Fig. 3. Reference designs: (a) distribution on the f/ε plane, and (b) designs allocated in a three-dimensional space. The shaded area is a manifold that determines the region of interest for surrogate model construction [42].
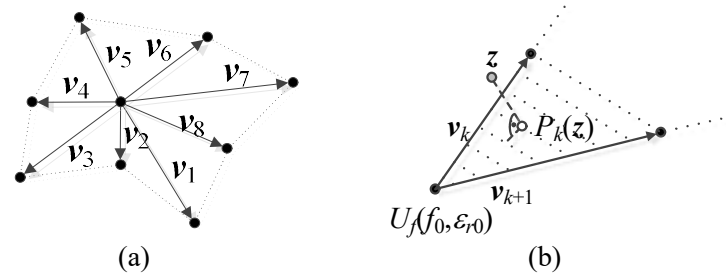
Fig. 4. Surrogate model domain defining components: (a) the manifold of Fig. 3(b) with the spanning vectors v_k marked; (b) manifold M_k with its spanning vectors and a point z and its projection onto the hyper-plane containing M_k [42].

The presented concept can be generalized in a straightforward manner; however, as the number of reference designs grow very quickly with the number of operating conditions considered (here, two), a practical application of the approach is limited to a few conditions.

The surrogate model is constructed using kriging interpolation of the EM model response R based on the training data sampled within X_S [42]. The design of experiments is based on random sampling within the interval $[x_{min}, x_{max}]$ assuming uniform probability distribution. The samples allocated outside $[x_{min}, x_{max}]$ are rejected.

3.2. Case Study: Ring Slot Antenna

A ring slot antenna shown of Fig. 5 [47] is used for demonstration purposes. The structure comprises a microstrip line that feeds a circular ground plane slot with defected ground structure (DGS). The thickness of the substrate is 0.762 mm. The parameter set is: $x = [l_f\ l_d\ w_d\ r\ s\ s_d\ o\ g\ \varepsilon_r]^T$; ε_r represents relative permittivity of the substrate. The feed line width w_f is computed for each ε_r to ensure 50 ohm input impedance. The computational model of the antenna is implemented in CST (~300,000 cells, simulation 90 s).

The antenna is supposed to be modeled within wide ranges of operating conditions: f_{min} = 2.5 GHz to f_{max} = 6.5 GHz (operating frequency), and ε_{min} = 2.0 to ε_{max} = 5.0 (substrate permittivity). The reference designs have been obtained by optimizing the structure of Fig. 5 for all combinations of $f \in$ {2.5, 4.5, 6.5} GHz and $\varepsilon_r \in$ {2.0, 3.5, 5.0} using feature-based optimization (FBO) [48]. Optimization is understood as minimizing the antenna reflection at f_0.

The model has been set up for d_{max} = 0.2 using 100, 200, 500 and 1000 random samples. The test set contained 100 random points. For benchmarking, the kriging model was also constructed using 1000 training points allocated in a conventional domain $X =$ [x_{min}, x_{max}]. Table 1 shows the average RMS errors for all considered models. Selected two-dimensional projections of the training sets for uniform and constrained sampling are shown in Fig. 6. The performance-driven surrogate allows for 3.5-fold improvement of the predictive power. At the same time, comparable modeling error is achieved with ten-fold reduction of the number of training samples. Figure 7 shows the surrogate and EM model responses at the selected test designs.
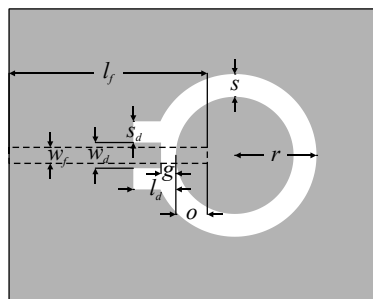

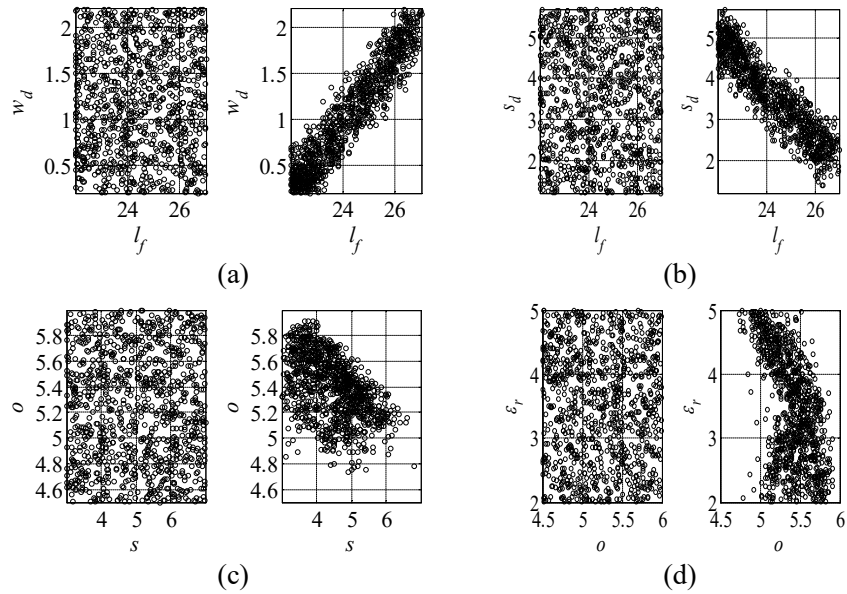Fig. 5. Geometry of the ring slot antenna [47].

Fig. 6. Uniform versus constrained sampling for selected two-dimensional projections onto (a) l_f-w_d plane, (b) l_f-s_d plane, (c) s-o plane, and (d) o-ε_r plane [42].
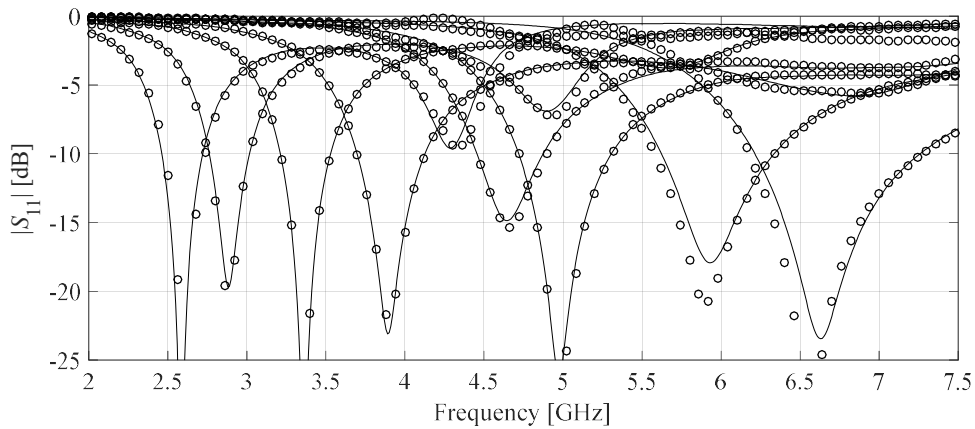
Fig. 7. Responses of the antenna of Fig. 5 at the selected test designs for $N = 1000$: high-fidelity EM model (—), performance-driven surrogate model (o) [42].

Table 1. Ring slot antenna: modeling results

Design Space Sampling and Surrogate Modeling Technique*	Average Relative RMS Error
Uniform sampling in the original space, $N = 1000$	7.3 %
Constrained sampling, $N = 100$	7.8 %
Constrained sampling, $N = 200$	5.5 %
Constrained sampling, $N = 500$	3.3 %
Constrained sampling, $N = 1000$	2.1 %

* In all cases, the surrogate model constructed using kriging interpolation [28].

4. Triangulation-Based Modeling

Triangulation-based performance-driven modeling [43] can be considered as a generalization of the method of Section 3. It permits arbitrary allocation of the reference designs and it is formulated to handle (at least in principle) an arbitrary number of operating conditions.

4.1. Modeling Framework

We use the same notation concerning the parameter and objective space as introduced in Section 2. In particular, the surrogate model is constructed in the region spanned by the reference designs $\boldsymbol{x}^{(j)} = [x_1^{(j)} \ldots x_n^{(j)}]^T$, $j = 1, \ldots, p$, optimized for selected objective vectors $\boldsymbol{f}^{(j)} = [f_1^{(j)} \ldots f_N^{(j)}]^T$. The reference designs are assigned to a set of simplexes using Delaunay triangulation [49]. The sets of vertices of the simplex $S^{(k)}$, $k = 1, \ldots, N_S$, is denoted as $S^{(k)} = \{\boldsymbol{x}^{(k.1)}, \ldots, \boldsymbol{x}^{(k.N+1)}\}$, where $\boldsymbol{x}^{(k.j)} \in \{\boldsymbol{x}^{(1)}, \ldots, \boldsymbol{x}^{(N)}\}$, $j = 1, \ldots, N + 1$, are individual vertices. The triangulation process is illustrated in Fig. 8.

$$S^{(1)} = [\boldsymbol{x}^{(1)}\,\boldsymbol{x}^{(2)}\,\boldsymbol{x}^{(4)}] \qquad S^{(4)} = [\boldsymbol{x}^{(2)}\,\boldsymbol{x}^{(5)}\,\boldsymbol{x}^{(7)}] \qquad S^{(7)} = [\boldsymbol{x}^{(5)}\,\boldsymbol{x}^{(6)}\,\boldsymbol{x}^{(8)}]$$
$$S^{(2)} = [\boldsymbol{x}^{(1)}\,\boldsymbol{x}^{(3)}\,\boldsymbol{x}^{(4)}] \qquad S^{(5)} = [\boldsymbol{x}^{(2)}\,\boldsymbol{x}^{(4)}\,\boldsymbol{x}^{(6)}] \qquad S^{(8)} = [\boldsymbol{x}^{(6)}\,\boldsymbol{x}^{(7)}\,\boldsymbol{x}^{(8)}]$$
$$S^{(3)} = [\boldsymbol{x}^{(2)}\,\boldsymbol{x}^{(5)}\,\boldsymbol{x}^{(6)}] \qquad S^{(6)} = [\boldsymbol{x}^{(4)}\,\boldsymbol{x}^{(6)}\,\boldsymbol{x}^{(7)}] \qquad S^{(9)} = [\boldsymbol{x}^{(5)}\,\boldsymbol{x}^{(8)}\,\boldsymbol{x}^{(9)}]$$
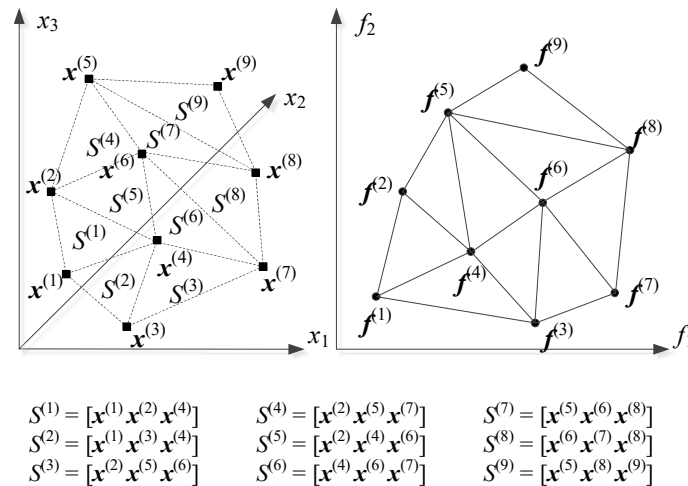
Fig. 8. Triangulation-based modeling: reference designs and their triangulation (left plot) and objective vectors corresponding to the reference designs (right plot). In the example shown, we have $N = 2$ (two figures of interest), $p = 9$ (nine reference designs), and $N_S = 9$ (nine simplexes).

The surrogate model domain X_S is determined as a vicinity of the manifold M being the union of the simplexes $S^{(k)}$, i.e.,

$$M = \bigcup_k \{ y = \sum_{j=1}^{N+1} \alpha_j x^{(k.j)} : 0 \leq \alpha_j \leq 1, \sum_{j=1}^{N+1} \alpha_j = 1 \} \tag{6}$$

The vicinity is determined by the distance from M in the orthogonal complements of the subspaces containing $S^{(k)}$. To determine whether a given point z belongs to the domain, the distance between z and the manifold M must be found. For that, consider a projection $P_k(z)$ of a point z onto the hyper-plane H_k containing $S^{(k)}$. For further use, we define the simplex anchor $x^{(0)} = x^{(k.1)}$, and its spanning vectors $v^{(j)} = x^{(k.j+1)} - x^{(0)}$, $j = 1, \ldots,$ N (cf. Fig. 9(a)). The projection corresponds to the expansion coefficients w.r.t. $v^{(j)}$ [43]

$$\arg \min_{[\bar{\alpha}^{(1)}, \ldots, \bar{\alpha}^{(N)}]} \left\| z - \left[x^{(0)} + \sum_{j=1}^{N} \bar{\alpha}^{(j)} \bar{v}^{(j)} \right] \right\|^2 \tag{7}$$

where the vectors $\bar{v}^{(j)}$ are obtained from $v^{(j)}$ by orthogonalization (i.e., $\bar{v}^{(1)} = v^{(1)}$, $\bar{v}^{(2)} = v^{(2)} - a_{12} v^{(1)}$ where $a_{12} = v^{(1)T} v^{(2)} (v^{(1)T} v^{(1)}$, etc.). In general

$$\bar{V} = \left[\bar{v}^{(1)} \; \bar{v}^{(2)} \; \ldots \bar{v}^{(N)} \right] = \left[v^{(1)} \; v^{(2)} \; \ldots v^{(N)} \right] A \tag{8}$$

Here, A is an upper-triangular matrix of coefficients obtained from the above orthogonalization procedure. The problem (7) is equivalent to

$$\left[\bar{v}^{(1)} \; \bar{v}^{(2)} \; \ldots \bar{v}^{(N)} \right] \begin{bmatrix} \bar{\alpha}^{(1)} \\ \vdots \\ \bar{\alpha}^{(N)} \end{bmatrix} = z - x^{(0)} \tag{9}$$

As the dimension of the simplex is normally lower than the dimension of the design space, the expansion coefficients can be found as follows

$$\begin{bmatrix} \bar{\alpha}^{(1)} \\ \vdots \\ \bar{\alpha}^{(N)} \end{bmatrix} = (\bar{V}^T \bar{V})^{-1} \bar{V}^T (z - x^{(0)}) \tag{10}$$

To determine whether $P_k(\mathbf{z})$ is within the convex hull of the simplex $S^{(k)}$, one needs the expansion coefficients $\alpha^{(j)}$ of $\mathbf{z}$ with respect to the original vectors $\mathbf{v}^{(j)}$, which can be found as $[\alpha^{(1)} \ldots \alpha^{(N)}]^T = A[\bar{\alpha}^{(1)} \ldots \bar{\alpha}^{(N)}]^T$. Further, $P_k(\mathbf{z}) \in S^{(k)}$ if and only if it is a convex combination of the vectors $\mathbf{v}^{(j)}$, i.e., if the following two conditions are satisfied:

1. $\alpha^{(j)} \geq 0$ for $j = 1, \ldots, N$, and

2. $\alpha^{(1)} + \ldots + \alpha^{(N)} \leq 1$.

In the next step we define $\mathbf{x}_{\max} = \max\{\mathbf{x}^{(k)}, k = 1, \ldots, p\}$ and $\mathbf{x}_{\min} = \min\{\mathbf{x}^{(k)}, k = 1, \ldots, p\}$. The vector $\mathbf{dx} = \mathbf{x}_{\max} - \mathbf{x}_{\min}$ determines the range of variation of geometry parameters of a device at hand within M. The domain X_S of the surrogate is defined similarly as in [42], by the following two conditions: a vector $\mathbf{y} \in X_S$ if and only if

1. The set $K(\mathbf{y}) = \{k \in \{1,\ldots,N_S\} : P_k(\mathbf{y}) \in S^{(k)}\}$ is not empty;

2. $\min\{\|(\mathbf{y} - P_k(\mathbf{y}))//\mathbf{dx}\|_\infty : k \in K(\mathbf{y})\} \leq d_{\max}$ (// denotes component-wise division; $d_{\max}$ is a user-defined parameter.

The geometric interpretation of these conditions can be found in [43]. The size of the model domain can be controlled by $d_{\max}$ (see Fig. 9(b) for graphical illustration).
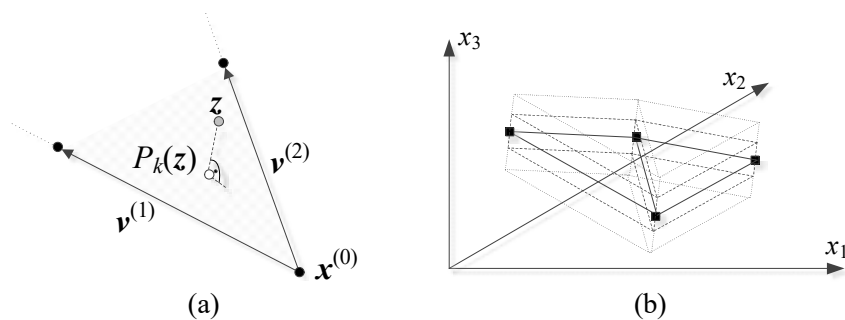

Fig. 9. (a) An example simplex $S^{(k)}$ with its anchor and the spanning vectors. Also shown are a point $\mathbf{z}$ and its projection onto the hyper-plane H_k containing $S^{(k)}$; (b) The meaning of thickness parameter $d_{\max}$ for a three-dimensional design space: reference designs (black squares), simplexes (—), along with two surrogate model domains, corresponding to the smaller (- - -) and larger (····) $d_{\max}$.

Note that $M \subset X_S$ by definition. For typical values of d_{max} of 0.05 to 0.2, the size of X_S is significantly smaller than the size of the parameter space X (i.e., here, the interval $[x_{min}, x_{max}]$). This allows for a considerable reduction of the number of samples necessary for surrogate model construction. At the same time, X_S contains the designs that are optimum w.r.t. the selected figures of interest, and, assuming sufficient regularity of the device responses w.r.t. its geometry parameters, the optimum designs for all combinations of the same figures of interest within the convex hull of $f^{(j)}$, $j = 1, \ldots, N$. Consequently, using a fraction of samples required by the conventional model, one can render a surrogate valid over a wide range of geometry/material parameters of the structure as demonstrated in the next section.

4.2. Verification Case Study: Dual-Band Uniplanar Dipole Antenna

Consider a dual-band uniplanar dipole antenna shown in Fig. 10(a) [50], implemented on RF-35 substrate ($\varepsilon_r = 3.5$, $h = 0.762$ mm) and fed by a 50 Ohm coplanar waveguide (CPW). The design parameters are: $x = [l_1\ l_2\ l_3\ w_1\ w_2\ w_3]^T$, whereas $l_0 = 30$, $w_0 = 3$, $s_0 = 0.15$ and $o = 5$ are fixed (all dimensions in mm). The EM antenna model R (~100,000 cells; simulation time 60 seconds) is implemented in CST Microwave Studio.

The goal is to build the surrogate for the following ranges of operating frequencies 2.0 GHz $\leq f_1 \leq$ 4.0 GHz (lower band), and 4.5 GHz $\leq f_2 \leq$ 6.5 GHz (upper band). Figure 10(b) shows the allocation of the reference designs selected for this example. The lower and upper bounds for design variables were set using the reference designs as $l = [25.0\ 6.0\ 14.0\ 0.2\ 1.6\ 0.5]^T$, and $u = [35.0\ 15.0\ 21.0\ 0.55\ 4.0\ 2.0]^T$. The reference design were obtained using feature-based optimization framework with variable-fidelity EM models [48].

The surrogate model has been constructed for d_{max} = 0.05 using kriging interpolation surrogate and training sets of various sizes: 100, 200, 400, 800, and 1600 random samples. Figure 11 shows selected two-dimensional projections of the constrained sampling. The model accuracy has been verified using 100 independent test points. Table 2 reports the average RMS errors for the triangulation-based model and conventional kriging surrogate. Computational benefits of performance-driven approach are evident. Figure 12 shows the surrogate and EM model responses at the selected test designs.

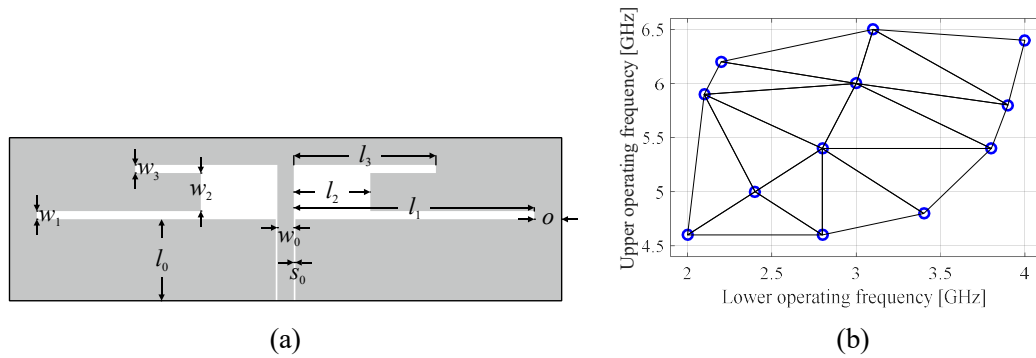(a)   (b)

Fig. 10. Uniplanar dipole antenna: (a) geometry [50], (b) allocation of the reference designs and their triangulation [43].
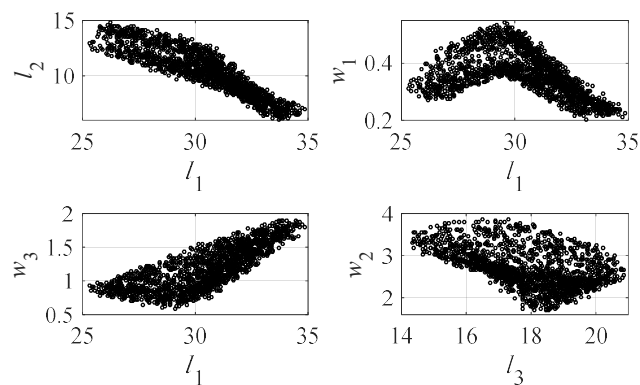

Fig. 11. Constrained sampling for selected two-dimensional projections onto l_1-l_2 plane, l_1 −w_1 plane, l_1-w_3 plane, and l_3-w_2 plane [43].
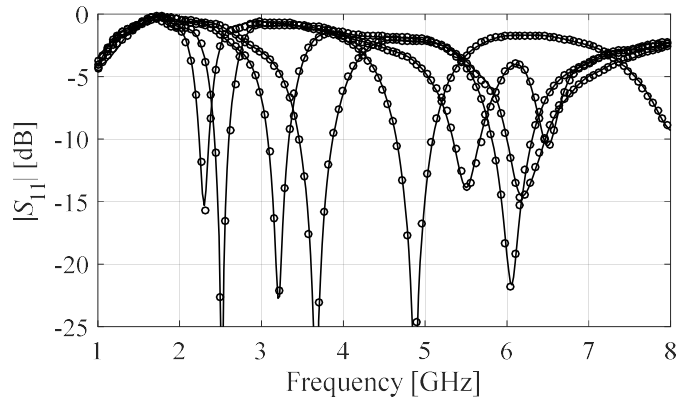
Fig. 12. Responses of the uniplanar dipole antenna of Fig. 10(1) at the selected test designs for $N = 1600$: high-fidelity EM model (—), triangulation-based surrogate (o).

Table 2: Uniplanar dipole antenna: modeling results

Number of training samples[#]	Relative RMS Error[*]	
	Conventional surrogate[$]	Triangulation-based surrogate
100	17.2 %	4.6 %
200	12.7 %	3.5 %
400	9.3 %	2.8 %
800	6.9 %	2.6 %
1600	5.7 %	2.3 %

[*] In all cases, the surrogate model constructed using kriging interpolation.
[#] The cost of finding the reference designs for constrained modeling is about 400 evaluations of the EM antenna model.
[$] Conventional surrogate established in the parameter space $X = [x_{min}, x_{max}]$.

5. Nested Kriging Modeling

The last technique discussed in this paper is nested kriging modeling [45] in which the surrogate model domain is defined using a separate kriging interpolation model. It is established using the reference designs and maps the objective space into the parameter space to provide the first approximation of the region of interest (i.e., containing high-quality designs). One of the major advantages of this approach is that design of experiments as well as surrogate model optimization can be realized in a convenient and straightforward manner.

5.1. Nested Kriging Modeling Procedure

The objective and parameter spaces are defined as in Section 2.1. Similarly as for the previously discussed techniques, the existence of reference designs $\boldsymbol{x}^{(j)} = [x_1^{(j)} \dots x_n^{(j)}]^T$, $j = 1, \dots, p$, is assumed. These are optimized with respect to the performance vectors $\boldsymbol{f}^{(j)} = [f_1^{(j)} \dots f_N^{(j)}]$ according to (1).

The nested kriging method utilized two surrogates. The first-level model $\boldsymbol{s}_I(\boldsymbol{f})$ maps the objective space F into the design space X. It is constructed using $\{\boldsymbol{f}^{(j)}, \boldsymbol{x}^{(j)}\}_{j=1,\dots,p}$ as the training set (see also Fig. 13).

The surrogate model is to be established within the region X_S that contains the designs which are optimum with respect to f_k, $k = 1, \dots, N$. As the first-level model is constructed using a discrete set of points optimal in the sense of (1), the image $\boldsymbol{s}_I(F) \subset X$ only provides an approximation of $U_f(\boldsymbol{f})$. In order to ensure that the domain X_S contains the entire manifold $U_f(\boldsymbol{f})$ (or a vast majority of it), $\boldsymbol{s}_I(F)$ must be enlarged. This, within the nested kriging framework is realized by an orthogonal extension of $\boldsymbol{s}_I(F)$ towards its normal vectors. We denote by $\{\boldsymbol{v}_n^{(k)}(\boldsymbol{f})\}$, $k = 1, \dots, n - N$, an orthonormal basis of vectors normal to $\boldsymbol{s}_I(F)$ at $\boldsymbol{f}$, and define $\boldsymbol{x}_{\max} = [x_{\max.1} \dots x_{\max.n}]^T$, $\boldsymbol{x}_{\min} = [x_{\min.1} \dots x_{\min.n}]^T$, with $x_{\max.k} = \max\{x_k^{(j)}, j = 1, \dots, p\}$, and $x_{\min.k} = \min\{x_k^{(j)}, j = 1, \dots, p\}$. We also define $\boldsymbol{x}_d = \boldsymbol{x}_{\max} - \boldsymbol{x}_{\min}$ (parameter variations within $\boldsymbol{s}_I(F)$). Further, extension coefficients are defined as follows:

$$\boldsymbol{\alpha}(\boldsymbol{f}) = [\alpha_1(\boldsymbol{f}) \dots \alpha_{n-N}(\boldsymbol{f})]^T = 0.5 d_{\max} \left[|\boldsymbol{x}_d \boldsymbol{v}_n^{(1)}(\boldsymbol{f})| \ \dots \ |\boldsymbol{x}_d \boldsymbol{v}_n^{(n-N)}(\boldsymbol{f})| \right]^T \tag{11}$$

where $d_{\max}$ is a thickness parameter. The coefficients α_k determine the boundaries of X_S, located between the two manifolds (cf. Fig. 13(b)):

$$M_{\pm} = \left\{ \boldsymbol{x} \in X : \boldsymbol{x} = \boldsymbol{s}_I(\boldsymbol{f}) \pm \sum_{k=1}^{n-N} \alpha_k(\boldsymbol{f}) \boldsymbol{v}_n^{(k)}(\boldsymbol{f}) \right\} \tag{12}$$
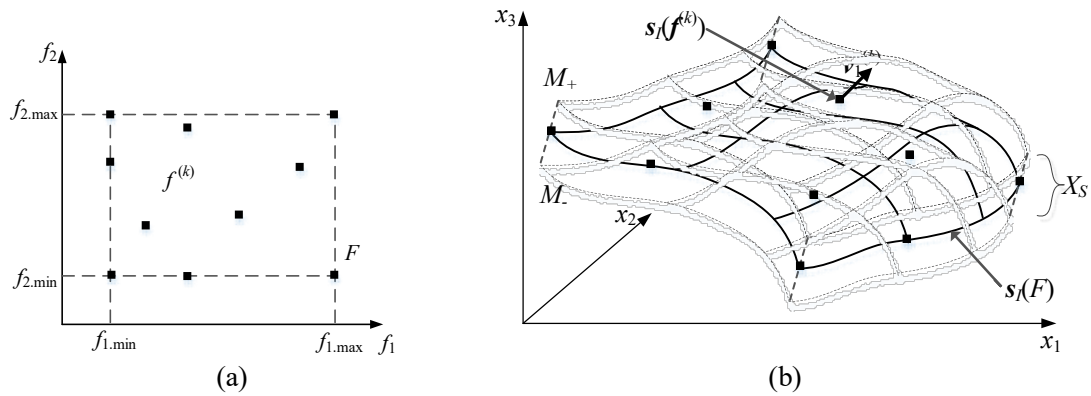
Fig. 13. The basic components of the nested kriging method: (a) reference designs and objective space F; (b) the image $s_I(F)$ of the first-level surrogate model, and the normal vector $v_1^{(k)}$ at $f^{(k)}$; the manifolds M_- and M_+ as well as the surrogate model domain X_S defined as orthogonal extension of $s_I(F)$ [46].

This can be formally written as

$$X_S = \left\{ \begin{matrix} \boldsymbol{x} = \boldsymbol{s}_I(\boldsymbol{f}) + \sum_{k=1}^{n-N} \lambda_k \alpha_k(\boldsymbol{f}) \boldsymbol{v}_n^{(k)}(\boldsymbol{f}) : \boldsymbol{f} \in F, \\ -1 \le \lambda_k \le 1, k = 1, \ldots, n-N \end{matrix} \right\} \quad (13)$$

The ultimate (or second-level) surrogate is a kriging model rendered in X_S based on a set of training points $\{\boldsymbol{x}_B^{(k)}, \boldsymbol{R}(\boldsymbol{x}_B^{(k)})\}_{k = 1, \ldots, N_B}$. Here, as usual, $\boldsymbol{R}$ denotes the EM-simulation model of the structure of interest.

It should be noted that the very definition of the set X_S facilitates design of experiments which was a problem for both [41] and [43]. It is implemented using (13) and the appropriate mappings from the unit interval $[0,1]^n$ onto X_S. Let $\{\boldsymbol{z}^{(k)}\}$, $k = 1, \ldots, N_B$, where $\boldsymbol{z}^{(k)} = [z_1^{(k)} \ldots z_n^{(k)}]^T$, denote the set of uniformly distributed data points in $[0,1]^n$ (here, using LHS [51]). The mapping is realized in two stages. First, the function h_1

$$\boldsymbol{y} = h_1(\boldsymbol{z}) = h_1([z_1 \ldots z_n]^T) = [f_{1.min} + z_1(f_{1.max} - f_{1.min}) \ldots f_{N.min} + z_N(f_{N.max} - f_{N.min})] \times \\ \times [-1 + 2z_{N+1} \ldots -1 + 2z_n] \quad (14)$$

transforms the unit hypercube onto a $F \times [-1,1]^{n-N}$ ($\times$ is a Cartesian product). The first N components of $\boldsymbol{y}$ correspond to original samples $\boldsymbol{z}$ uniformly distributed in the objective space, whereas the remaining $n - N$ components will be used to uniformly spread the samples in orthogonal directions defining X_S. Subsequently, a function h_2 is defined as

$$
\begin{aligned}
\boldsymbol{x} = h_2(\boldsymbol{y}) = h_2([y_1 \ldots y_n]^T) &= \boldsymbol{s}_I([y_1 \ \ldots \ y_N]^T) + \\
&+ \sum_{k=1}^{n-N} y_{N+k} \alpha_k([y_1 \ \ldots \ y_N]^T) \boldsymbol{v}_n^{(k)}([y_1 \ \ldots \ y_N]^T)
\end{aligned}
\tag{15}
$$

which maps $F \times [-1,1]^{n-N}$ onto X_S. Uniformly distributed samples $\boldsymbol{x}_B^{(k)}$ in X_S are obtained as

$$
\boldsymbol{x}_B^{(k)} = H(\boldsymbol{z}^{(k)}) = h_2(h_1(\boldsymbol{z}^{(k)}))
\tag{16}
$$

Note that the first component of mapping h_2, i.e., $\boldsymbol{s}_I(\boldsymbol{y})$, places the sample on the manifold $\boldsymbol{s}_I(F)$, whereas the second component shifts the sample in orthogonal directions $\boldsymbol{v}_n^{(k)}$ so that the samples fill the entire domain X_S. The function H can also be used for other purposes, in particular, parametric optimization of the surrogate within X_S. As H is surjective, it is sufficient to operate within $F \times [-1,1]^{n-N}$ regardless of X_S geometry and to only apply (16) to perform evaluation of the structure under design.

5.2. Illustration Example: Miniaturized Impedance Matching Transformer

The nested kriging method is demonstrated using a miniaturized 50-to-100 Ohm impedance matching transformer [52] shown in Fig. 14(b). The circuit is implemented on RF-35 substrate ($\varepsilon_r = 3.5$, $h = 0.762$ mm, $\tan \delta = 0.0018$) and utilizes compact microstrip resonant cells (CMRCs) of Fig. 14(a). The transformer geometry parameters are $\boldsymbol{x} = [l_{1.1}$ $l_{1.2} \ w_{1.1} \ w_{1.2} \ w_{1.0} \ l_{2.1} \ l_{2.2} \ w_{2.1} \ w_{2.2} \ w_{2.0} \ l_{3.1} \ l_{3.2} \ w_{3.1} \ w_{3.2} \ w_{3.0}]^T$.

The objective space is defined by the range of operating bands $[f_1\ f_2]$ with 1.5 GHz $\leq f_1 \leq 3.5$ GHz, and 4.5 GHz $\leq f_2 \leq 6.5$ GHz. Here, the optimum design is understood by minimization of the maximum reflection $|S_{11}|$ within $[f_1\ f_2]$ (which is a minimax problem). The allocation of the reference designs has been shown in Fig. 14(c). The lower and upper bounds for geometry parameters are $\boldsymbol{l}$ = [2.0 0.15 0.65 0.35 0.30 2.70 0.15 0.44 0.15 0.30 3.2 0.15 0.30 0.15 0.30]^T, and $\boldsymbol{u}$ = [3.4 0.50 0.80 0.55 1.90 4.00 0.50 0.67 0.50 1.55 4.5 0.26 0.46 0.27 1.75]^T.

For the sake of numerical verification, the nested kriging surrogate has been constructed for several training data sets of sizes 50, 100, 200, 400, and 800 samples. The thickness parameter has been set to d_{max} = 0.05. The predictive power of the model has been estimated using a set of 100 independent random test points. The numerical results are provided in Table 3 which shows the average RMS errors defined as $\|\boldsymbol{R}(\boldsymbol{x}) - \boldsymbol{R}_s(\boldsymbol{x})\|/\|\boldsymbol{R}(\boldsymbol{x})\|$, where $\boldsymbol{R}(\boldsymbol{x})$ and $\boldsymbol{R}_s(\boldsymbol{x})$ stand for the high-fidelity EM model and the surrogate, respectively. Conventional kriging and radial basis function surrogates (i.e., set up within the parameter space $X = [\boldsymbol{l}, \boldsymbol{u}]$) were included for comparison as well. Figure 15 shows the responses of the nested kriging surrogate and the EM model at selected test designs. A visual agreement between the two data sets is good.
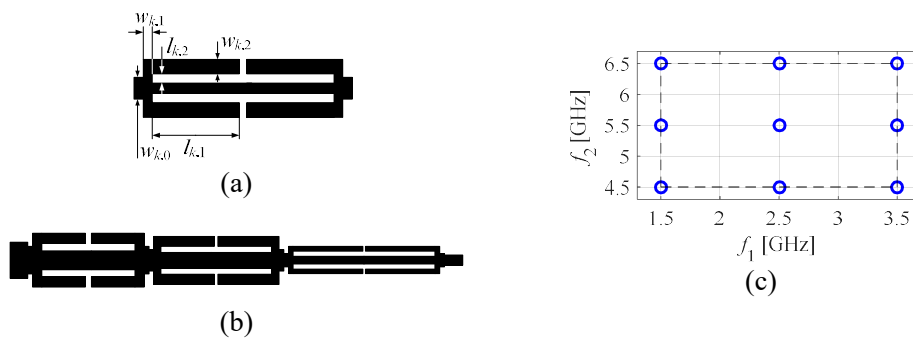

(a)

(b)

(c)

Fig. 14. Miniaturized impedance matching transformer: (a) compact cell (CMRC), (b) three-section transformer circuit [52], (c) allocation of the reference designs for the transformer [46].
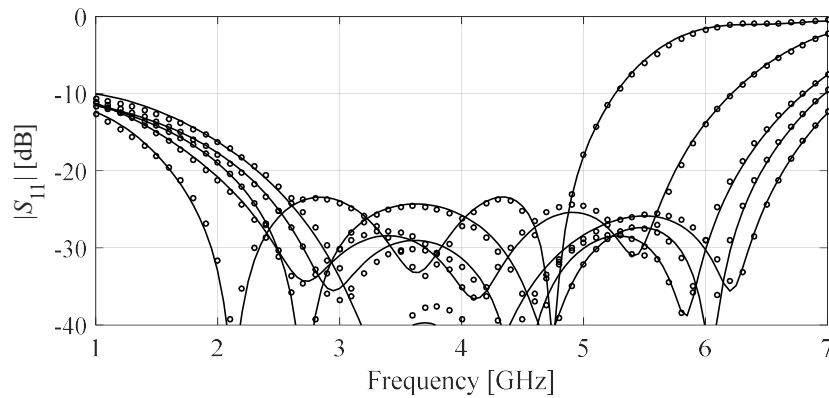
Fig. 15. Responses of the impedance transformer of Fig. 14(b) at the selected test designs for $N = 800$: EM model (—), proposed nested kriging surrogate (o) [46].

Table 3. Modeling Results and Benchmarking for RRC and Transformer

Number of training samples	Relative RMS Error		
	Conventional Models		Nested Kriging Model
	Kriging	RBF	
50	49.1 %	56.2 %	17.3 %
100	31.1 %	33.0 %	13.9 %
200	25.9 %	27.5 %	10.3 %
400	20.4 %	23.1 %	7.4 %
800	15.7 %	16.8 %	6.1 %

[$] Conventional surrogate established in the parameter space $X = [x_{min}, x_{max}]$.

The results of Table 1 indicate significant improvement of the predictive power (by a factor between two and three) of the nested kriging surrogate over that of the conventional one when the training data sets of the same sizes are compared. At the same time, conventional models require much larger data sets (by a factor of ten or higher) to reach the accuracy of the nested kriging model. Note that the accuracy of the conventional models is poor even for the largest data set consisting of 800 samples.

6. Discussion and Conclusion

This paper discussed the concept and recent developments of performance-driven surrogate modeling of high-frequency structures. As demonstrated using several examples of microwave and antenna components, confinement of the model domain to a region containing designs that are close-to-optimal with respect to performance figures of choice plays a crucial role in reducing the computational overhead related to acquisition of the training data. At the same time, it permits construction of reliable surrogates over wide ranges of geometry parameters and operating conditions. We discussed three particular implementations of this concept, different in how the model domain definition is formalized. The technique of Section 3 is the simplest in terms of formulation and implementation but it is limited in terms of allocation of the reference designs. Triangulation-based modeling of Section 4 is more flexible as it permits arbitrary placement of the reference set. It is also formulated to directly handle arbitrary number of operating conditions. The downside is a non-trivial design of experiments, although this issue has been addressed to a certain extent in follow-up works. The nested kriging framework is the most comprehensive of the three methods outlined in this paper, also in the sense that the mechanisms permitting uniform sampling and convenient surrogate model optimization are built into the model formulation. At the same time, this method is more complex implementation-wise than the techniques of Sections 3 and 4. Overall, the performance-driven concept can be viewed as an attractive alternative to conventional modeling methods, especially in cases where the latter fail due to dimensionality issues, nonlinearity of system outputs or wide ranges of parameters. In particular, the initial investment required to prepare the reference designs (if not already available) will pay off

if the surrogate is to be re-used on multiple occasions, e.g., to re-design a particular structure for various operating conditions, or when other techniques simply do not work.

Acknowledgement

References

1. Chaloun T, Ziegler V, Menzel W. Design of a dual-polarized stacked patch antenna for wide-angle scanning reflectarrays. *IEEE Trans Antennas Propag*. 2016;64(8):3380-3390.

2. Keerthi S, Hamad AH, Mian A, Clifford JJ, Majumdar PK, Chamok N, Ali M. Effect of heterogeneity in additively manufactured dielectric structures on RF response of microstrip patch antennas. *Int J RF Microw Comput Aided Eng*. 2018;28:e21234.

3. Wainwright G, Chen C. Low-profile broadband reflector antenna designed for low mutual coupling, *European Conf Ant Propag (EuCAP)*. 2016.

4. Koziel S, Unnsteinsson SD. Expedited design closure of antennas by means of trust-region-based adaptive response scaling. *IEEE Antennas Wirel Propag Lett*. 2018;17(6):1099-1103.

5. Torun HM, Swaminathan, M. High-dimensional global optimization method for

high-frequency electronic design. *IEEE Trans Microwave Theory Tech.* 2019;67(6):2128-2142.

6. Hosder S. Stochastic response surfaces based on non-intrusive polynomial chaos for uncertainty quantification. *Int J Num Model Num Optim*, 2012;3(1/2):117-139.

7. Ko J, Byun J, Park J, Kim H. Robust design of dual band/polarization patch antenna using sensitivity analysis and Taguchi's method. *IEEE Trans Magn.* 2011;47(5):1258-1261.

8. Booker AJ, Dennis JE, Frank PD, Serafini DB, Torczon V, Trosset MW. A rigorous framework for optimization of expensive functions by surrogates. *Struct Optim*. 1999;17:1-13.

9. Bandler JW, Cheng QS, Dakroury SA, Mohamed AS, Bakr MH, Madsen K, Søndergaard J. Space mapping: the state of the art. *IEEE Trans Microwave Theory Tech.* 2004;52(1):337-361.

10. Koziel S. Accurate low-cost microwave component models using shape-preserving response prediction. *Int J Num Model: Electr Devices Fields*. 2012;25(2):152-162.

11. Koziel S, Bekasiewicz A. Low-cost and reliable geometry scaling of compact microstrip couplers with respect to operating frequency, power split ratio, and dielectric substrate parameters. *IET Microw Ant Propag.* 2018;12(9):1508-1513.

12. Allaire G. A review of adjoint methods for sensitivity analysis, uncertainty quantification, and optimization in numerical codes. *Ing de l'Automobile, SIA*, 2015;836:33-36.

13. Ghassemi M, Bakr M, Sangary N. Antenna design exploiting adjoint sensitivity-based geometry evolution. *IET Microw Antennas Propag*, 2013;7(4):268-276.

14. Sóbester A, Forrester AIJ, Toal DJJ, Tresidder E, Tucker S. Engineering design applications of surrogate-assisted optimization techniques. *Optim Eng*. 2012;15(1):243-265.

15. Koziel S, Bekasiewicz A. Reliable multistage optimization of antennas for multiple performance figures in highly dimensional parameter spaces. *IEEE Ant Wireless Propag Lett.* 2019;18(7):1522-1526.

16. Bandler JW, Hailu DM, Madsen K, Pedersen F. A space-mapping interpolating surrogate algorithm for highly optimized EM-based design of microwave devices, *IEEE Trans Microwave Theory Techn.* 2004;52(11):2593-2600.

17. Ayed RB, Gong J, Brisset S, Gillon F, Brochet P. Three-level output space mapping strategy for electromagnetic design optimization. *IEEE Trans Magn.* 2012;48(2):671-674.

18. Koziel S, Leifsson L. *Simulation-driven design by knowledge-based response correction techniques*. Cham: Springer; 2016.

19. Koziel S, Bandler JW, Madsen K. Space mapping with adaptive response correction for microwave design optimization. *IEEE Trans Microwave Theory Tech.* 2009;57:478-486.

20. Koziel S, Bekasiewicz A. Fast simulation-driven feature-based design optimization of compact dual-band microstrip branch-line coupler. *Int J RF Microw Comput Aided Eng.* 2015;26(1):13-20.

21. Rasmussen CE, Williams CKI. *Gaussian processes for machine learning.* Cambridge: MIT Press, 2006.

22. Jin Y. A comprehensive survey of fitness approximation in evolutionary computation. *Soft Comput.* 2005;9(1):3-12.

23. Gorissen D, Dhaene T, De Turck F. Evolutionary model type selection for global surrogate modeling. *J Machine Learning Research.* 2009;(10):2039-2078.

24. Montegranario H, Espinosa J. *Radial basis functions*, In: *Variational regularization of 3D Data*, SpringerBriefs in Computer Science, New York: Springer, 2014.

25. Rayas-Sanchez JE. EM-based optimization of microwave circuits using artificial neural networks: the state-of-the-art. *IEEE Trans Microwave Theory Tech.* 2004;52(1):420-435.

26. Chávez-Hurtado JL, Rayas-Sánchez JE Polynomial-based surrogate modeling of RF and microwave circuits in frequency domain exploiting the multinomial theorem. *IEEE Trans Microwave Theory Tech.* 2016;64(12):4371-438.

27. Kitayama S, Arakawa M, Yamazaki K. Sequential approximate optimization using radial basis function network for engineering optimization. *Optim Eng.* 2011;12(4):535-557.

28. Kleijnen JPC. Kriging metamodeling in simulation: A review. *European J Operat Research.* 2009;192(3):707-716.

29. Angiulli G, Cacciola M, Versaci M. Microwave devices and antennas modelling by support vector regression machines. *IEEE Trans Magn.* 2007;43(4):1589-1592.

30. Jacobs JP. Efficient resonant frequency modeling for dual-band microstrip antennas by gaussian process regression. *IEEE Ant Wireless Propag Lett.* 2015;14:337-341.

31. Du J, Roblin C. Statistical modeling of disturbed antennas based on the polynomial chaos expansion. *IEEE Ant Wireless Prop Lett*, 2017;16:1843-1846.

32. Schobi R, Sudret B, Wiart J. Polynomial-chaos-based kriging. *Int J Uncertainty Quant*, 2015;5(2):171-193.

33. Wu X, Peng X, Chen W, Zhang W. A developed surrogate-based optimization framework combining HDMR-based modeling technique and TLBO algorithm for high-dimensional engineering problems. *Struct Multidisc Optim.* 2019;60(2):663-680.

34. Liu H, Hervas JR, Ong YS, Cai J, Wang Y. An adaptive RBF-HDMR modeling approach under limited computational budget. *Struct Multidisc Optim.* 2018;57(3):1-18.

35. Koziel S, Bekasiewicz A. Computationally feasible narrow-band antenna modeling using response features. *Int J RF Microw Comput Aided Eng.* 2017;27(4):e21077.

36. Tropp JA, Gilbert AC. Signal recovery from random measurements via orthogonal matching pursuit. *IEEE Trans Inf Theory.* 2007;53(12):4655-4666.

37. Bakr MH, Bandler JW, Madsen K, Rayas-Sanchez JE, Sondergaard J. Space-mapping optimization of microwave circuits exploiting surrogate models. *IEEE Trans Microwave Theory Tech*. 2000;48(12):2297-2306.

38. Wang F, Cachecho P, Zhang W, Sun S, Li X, Kanj R, Gu C. Bayesian model fusion: large-scale performance modeling of analog and mixed-signal circuits by reusing early-stage data, *IEEE Trans CAD Integr Circuits Systems.* 2016;35(8):1255-1268.

39. Koziel S, Ogurtsov S, Couckuyt I, Dhaene T. Variable-fidelity electromagnetic simulations and co-kriging for accurate modeling of antennas. *IEEE Trans Ant Propag.* 2013;61(3):1301-1308.

40. Jacobs JP, Koziel S. Two-stage framework for efficient gaussian process modeling of antenna input characteristics. IEEE Trans Ant Propag. 2014;62(2):706-713.

41. Koziel S. Low-cost data-driven surrogate modeling of antenna structures by constrained sampling. *IEEE Ant Wireless Prop Lett.* 2017;16:461-464.

42. Koziel S, Bekasiewicz A. On reduced-cost design-oriented constrained surrogate modeling of antenna structures. *IEEE Ant Wireless Prop Lett.* 2017;16:1618-1621.

43. Koziel S, Sigurðsson AT. Triangulation-based constrained surrogate modeling of antennas. *IEEE Trans Ant Propag.* 2018;66(8):4170-4179.

44. Koziel S, Sigurðsson AT, Szczepanski S. Uniform sampling in constrained domains for low-cost surrogate modeling of antenna input characteristics, *IEEE Ant Wireless Prop Lett.* 2018;17(1):164-167.

45. Koziel S, Pietrenko-Dabrowska A. Performance-based nested surrogate modeling of antenna input characteristics, *IEEE Trans Ant Propag.* 2019;67(5):2904-2912.

46. Koziel S, Pietrenko-Dabrowska A. Reduced-cost surrogate modelling of compact microwave components by two-level kriging interpolation. *Eng Optim.* 2019; doi.org/10.1080/0305215X.2019.1630399.

47. Sim CYD, Chang MH, Chen BY. Microstrip-fed ring slot antenna design with wideband harmonic suppression. *IEEE Trans Ant Propag.* 2014;62(9):4828-4832.

48. Koziel S. Fast simulation-driven antenna design using response-feature surrogates. *Int J RF Microw Comput Aided Eng.* 2015;25(5):394-402.

49. Cheng SW, Dey T, Shewchuk J. *Delaunay mesh generation*, New York: Chapman and Hall; 2013.

50. Chen YC, Chen SY, Hsu P. Dual-band slot dipole antenna fed by a coplanar waveguide. *IEEE Int Symp Ant Propag.* 2006.

51. Ai M, Kong X, Li K. A general theory for orthogonal array based latin hypercube sampling. *Statistica Sinica*. 2016;26(2):761-777.

52. Koziel S, Bekasiewicz A. Rapid simulation-driven multi-objective design optimization of decomposable compact microwave passives. *IEEE Trans Microwave Theory Techn.* 2016;64(8):2454-2461.